ACS OMEGA

Open Access



http://pubs.acs.org/journal/acsodf

Article

# The Development and Characterization of Two Monoclonal Antibodies Against the Conjugates and Derivatives of the Immunometabolite Itaconate

Lauren Switala, Lin Di, Simona Colantonio, Bindu Lakshman, Tessa W. Caceres, Joshua J. Reading, Sandra S. Garcia-Buntley, and Andrei Maiseyeu*

Cite This: *ACS Omega* 2025, 10, 1110−1121

Read Online

ACCESS | Metrics & More | Article Recommendations

**ABSTRACT:** We have developed two monoclonal antibodies, CPTC-2MeSC-1 and CPTC-2MeSC-2, against itaconate and its conjugates with sulfhydryl-containing biomolecules such as cysteines. Itaconate is a dicarboxylic acid metabolite that has recently gained much interest for its anti-inflammatory properties in many biological models. We have synthesized an itaconate−cysteine conjugate ITA-Cys designed to mimic in vivo Michael adducts of itaconate. Two monoclonal antibodies against ITA-Cys, CPTC-2MeSC-1 and CPTC-2MeSC, were developed and shown to have high immunoreactivity to unconjugated itaconate, itaconate−BSA conjugates, and Michael adducts of dimethyl itaconate. We found that CPTC-2MeSC-1 and CPTC-2MeSC-2 are specific and do not bind to other structurally similar cysteine Michael adducts, including those obtained from "sister" metabolites (fumarate, cis-aconitate), itaconate isomers (citraconate), and some itaconate esters. CPTC-2MeSC-2 is a useful tool in both studying biological actions of itaconate and developing therapeutic applications of itaconate and its derivatives.

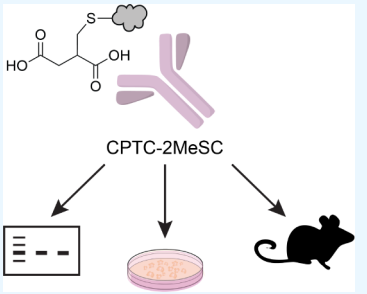


## INTRODUCTION

Itaconic acid (itaconate) is a metabolite formed as an intermediate product of the tricarboxylic acid (TCA) cycle, first isolated by Samuel Baup in 1836 while studying the decomposition of citric acid.[1−3] In mammalian systems, it is formed intracellularly through decarboxylation of the TCA intermediate *cis*-aconitate in a cataplerotic reaction via the enzyme aconitate decarboxylase 1 (ACOD1, encoded by the gene Acod1), alternatively known as immunoresponsive gene 1 (gene: Irg1).[4]

The biological functions of itaconates are numerous. Initial interest in the molecule revolved around its antibacterial properties, including its inhibition of*Pseudomonas indigofera*-growth and its response to*Mycobacterium tuberculosis* infection.[5,6] More recently, itaconate has been shown to exhibit anti-inflammatory properties in various contexts and has been demonstrated to be produced by activated macrophages.[7−9] Anti-inflammatory properties of itaconate have been initially linked to a plethora of mechanisms, such as inhibition by competitive binding of succinate dehydrogenase (SDH), which catalyzes the oxidation of succinate to fumarate, and, if overproduced, generates mitochondrial reactive oxygen species (mROS).[10,11] Another known mechanism by which itaconate inhibits inflammation is through activating nuclear factor erythroid 2-related factor 2 (NRF2), a transcription factor responsible for antioxidant and anti-inflammatory responses in the cell, via proteasomal degradation of Kelch-like ECH-associated protein 1 (Keap1).[8,12] Furthermore, itaconate combats inflammation by electrophilic stress placed on IκBζ, whose inhibition upregulates anti-inflammatory-activating transcription factor 3 (ATF3). This mechanism is more pronounced in itaconate's more electrophilic derivatives than itaconate itself.[13]

Many of the aforementioned biological mechanisms of action of itaconate rely on the molecule's electrophilic properties. As such, itaconate's methylene group in the $\alpha$ position constitutes a classic Michael acceptor able to engage in addition reactions with thiols such as cysteines of proteins or glutathione (Figure 1A).[8] For instance, the aforementioned activation of NRF2 has been shown to occur via proteasomal degradation of Keap1, an inhibitor of NRF2, after alkylation of cysteine residues by itaconate.[8] A significant portion of work elucidating itaconate's mechanisms has been done using its esterified derivatives such as dimethyl itaconate (DMI) and octyl itaconate (OI).[14] In these more electrophilic derivatives, the methylene group is more reactive and these molecules produce biological effects distinct from those of itaconate.[13] While these derivatives have been initially used to probe the

Received: September 17, 2024
Revised: December 4, 2024
Accepted: December 10, 2024
Published: December 20, 2024

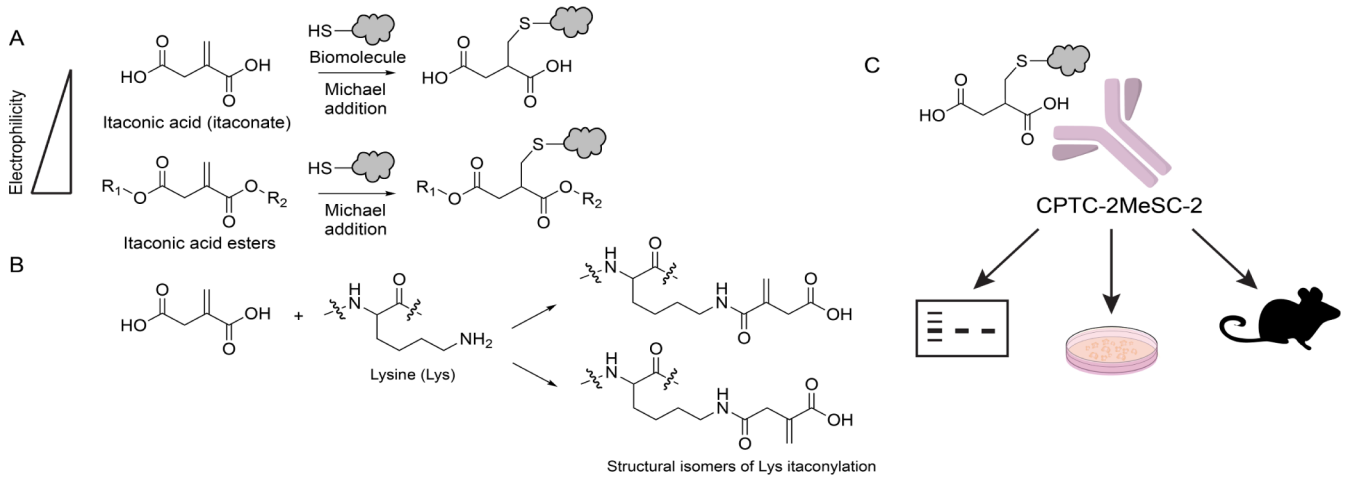


**Figure 1.** Design considerations in the development of an antigen mimicking Michael adducts of itaconate. (A) Itaconate and its ester derivatives are classic Michael acceptors able to react with sulfhydryl groups of biomolecules. The electrophilicity of itaconic acid is lower than that of its mono- and diesters. (B) Alternative vision for itaconate conjugates is lysine modification through a peptide bond that would result in two possible structural isomers (regioisomers). (C) A monoclonal antibody, CPTC-2MeSC-2, against itaconate−cysteine conjugates is a promising tool for numerous in vitro and in vivo applications.

biology of itaconate, numerous recent reports demonstrated their therapeutic actions against various pathologies.[8,15] Because of its immunometabolic actions across organ systems and disease models, as well as a far reaching promise of itaconate-based therapies,[5−9] a reliable, inexpensive, and robust method of itaconate conjugates' identification is urgently needed.

However, detection of a small molecule metabolite within the myriad substances present in biological substances is a challenging task, particularly in light of itaconate's biochemistry. Given the reactivity of itaconate and its derivatives due to their electrophilicity, it stands to reason that these molecules do not typically exist freely intracellularly but rather in the form of conjugates with various thiols including cysteine-rich proteins. For instance, Bambouskova et al. demonstrated that both exogenous DMI and endogenous itaconate covalently conjugate to glutathione (GSH).[13] Similarly, O'Neill and colleagues determined that itaconate directly modifies proteins via alkylation of cysteine residues.[8] In developing detection methods for itaconate, both in studying endogenous biological activity and in assessing the efficacy of itaconate-based therapies, covalent conjugation must be taken into consideration. Mass spectrometry (MS) is a mainstay in the detection of metabolites, including various metabolite-mediated post-translational modifications (PTMs). MS has been previously successfully utilized for highly accurate itaconate detection both in its free, unconjugated form and for itaconate PTMs.[16−19] However, MS requires specialized technical expertise and high-maintenance instrumentation and is burdened with high operational costs. This may be prohibitive for low-resource settings. Furthermore, for each therapeutic formulation of itaconate screened, a new MS method must be developed in accordance with the relevant conjugates formed, which is time-consuming and increases the cost. This process becomes even more challenging for detection in complicated matrices, such as tissue sections or whole organisms. As such, analytical characterization of novel formulations has remained the main limitation in therapeutic development. Alternative methods have been developed, including indirect detection of itaconate by cysteine profiling[20] and competitive cysteine binding.[21] Separately, a biosensor called "BioITA" was reported to detect intracellular itaconate with subcellular resolution.[22] Although potentially useful in studying biological action, this tool's applicability would be challenged in measuring the accumulation of novel therapeutics, particularly since the itaconate-conjugate phenomenon has not been addressed with this tool.

The work presented in this article showcases two new monoclonal antibodies, CPTC-2MeSC-1 and CPTC-2MeSC-2, generated against itaconate−cysteine conjugates for use in analytical characterization of therapeutic applications. We demonstrate that one of these antibodies, CPTC-2MeSC-2, binds to exogenous and endogenous itaconates and their derivatives under a variety of conditions. CPTC-2MeSC-2 is suitable for different detection methods both in vitro and in vivo, including Western blot and tissue and cellular immunohistochemistry (IHC). To mimic pertinent itaconate-protein Michael conjugates, we developed an itaconate conjugate, ITA-Cys, for which both CPTC-2MeSC-1 and CPTC-2MeSC-2 show high affinity. Additionally, CPTC-2MeSC-2 allows detection of in vivo accumulation of an itaconate derivative using standard techniques. CPTC-2MeSC-2 fulfills an analytical need in researching this fascinating metabolite with far-reaching therapeutic potential (Figure 1C).

## RESULTS

Our approach began with the synthesis of an itaconate-based antigen to be utilized for animal immunization and hybridoma production. Design of the antigen considered two major points: (1) it should represent itaconate cysteine conjugates, similar to Michael adducts that have been previously demonstrated to form in vivo as a result of protein cysteine alkylation by the itaconate and its ester derivatives (Figure 1A), which we termed as 2-methyl-succination, and (2) alternative designs of the antigen representing posttranslational modification via the epsilon amino group of lysine residues (Figure 1B) were less relevant and are more challenging to generate as lysine itaconylation can produce two distinct structural isomers (Figure 1B). Thus, we focused on the production of (2*S*)-2-methylsuccinyl-cysteine and the two


https://doi.org/10.1021/acsomega.4c08552
*ACS Omega* 2025, 10, 1110−1121

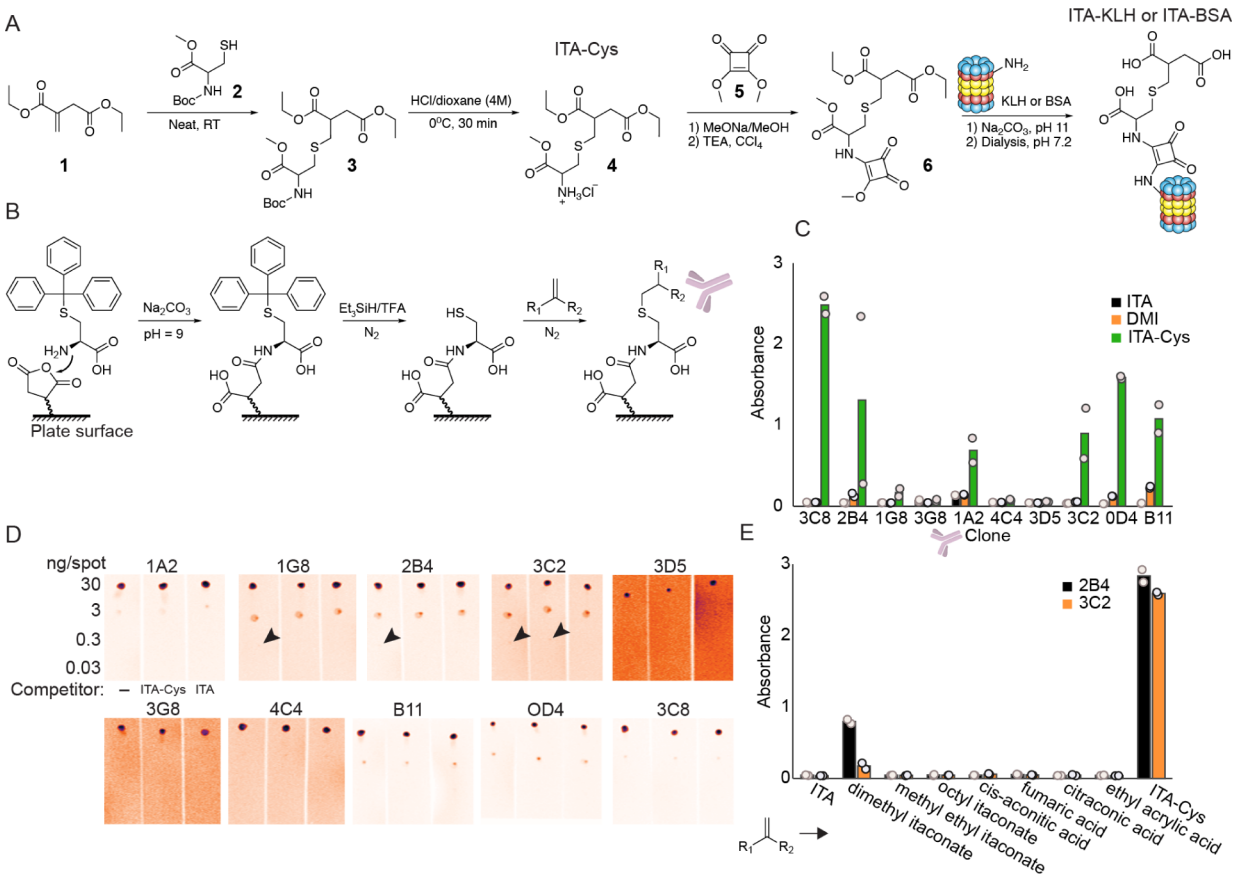


**Figure 2.** Screening of 10 monoclonal antibody clones resulted in the selection of 2 candidates for further validation. (A) Synthesis scheme of ITA-Cys and its subsequent conjugation to KHL or BSA. (B) Schematic of ELISA for itaconate analog binding, illustrating chemistry used to attach structurally similar molecules to a maleic anhydride plate via bound cysteine. (C) ELISA results for all 10 CPTC-2MeSC clones, binding to itaconate (black), dimethyl itaconate (DMI, orange), and itaconate-cysteine conjugate (ITA-Cys, green). (D) Dot blot for all 10 clones, binding to ITA-BSA at varying concentrations per spot. Arrowheads point to a detected signal from 0.3 ng/spot ITA-BSA. (E) ELISA results for top 2 clone candidates (2B4 [black] and 3C2 [orange]), binding to various Michael adducts of molecules structurally similar to itaconate.

antibodies recognizing this antigen were termed CPTC-2MeSC-1 and CPTC-2MeSC-2.

For the synthesis of Michael adduct 4 (ITA-Cys), Boc deprotection in a one-pot two-step synthetic strategy of commercially available diprotected cysteine derivative (Cys-Boc-OMe) and the use of diethyl itaconate both as a reactant and a solvent (Figure 2A) resulted in Michael adduct 4 as an amine ester. Squaric acid chemistry was then used to prepare conjugates in two steps. The reaction of squaric acid dimethyl ester 5 with amine 4 in organic solvent led to the formation of the squaric acid monoester monoamide 6. Finally, squaric acid diamide conjugates with required carrier proteins keyhole limpet hemocyanin (KLH) or bovine serum albumin (BSA) were formed in aqueous solutions at pH 11. The latter step also aided in hydrolysis to yield de-esterified conjugates. After buffer exchange and sterile filtration, two antigens ITA-KLH and ITA-BSA were ready for downstream application. Antigens were provided to OriGene Technologies Inc. for mouse antibody development. ITA-KLH was used for animal immunization and ITA-BSA was employed as a standard for immunoreactivity testing in multiple applications including indirect ELISA. Under OriGene's streamlined mouse monoclonal antibody production pipeline, including immunization and serum development, splenectomy, and hybridoma selection, 10 unique clones with high immunoreactivity toward ITA-BSA and ITA-Cys (titers 70,000−650,000) were identified and expanded.

2-Methyl-succination is structurally similar to other possible cysteine Michael adducts that can occur in biological systems, including fumarate-induced cysteine succination[23] and mesaconate/citraconate adducts.[24] We developed a screening platform schematically shown in Figure 2B to test for specificity of the antibody clones to 2-methyl-succination versus a number of structurally similar motifs. A maleic-anhydride-coated plate was first treated with *S*-trityl-cysteine, which was then deprotected with triethylsilane in trifluoroacetic acid under an inert atmosphere. In a proof-of-concept experiment, the resulting plate-bound cysteine was first reacted with unmodified itaconic acid (ITA) and dimethyl itaconate (DMI). A plate bound with ITA-Cys served as a positive control (Figure 2C). All 10 clones were then screened in this assay for immunoreactivity. Six out of ten antibodies produced immunoreactive signal in this assay (SNR of itaconate = 14.4, DMI = 15.2, ITA-Cys = 8.8), with the ITA-Cys resulting in the highest amount of binding, likely because it more closely mimics the state of the inoculating itaconate (ITA-Cys conjugated to KLH) than the unconjugated form or DMI. Further screening of the 10 clones was performed using a dot blot against ITA-BSA at a range of concentrations of 30−0.03 ng/spot (Figure 2D). In this assay, ITA-Cys and ITA were additionally used in a large excess at the time of


https://doi.org/10.1021/acsomega.4c08552
ACS Omega 2025, 10, 1110−1121

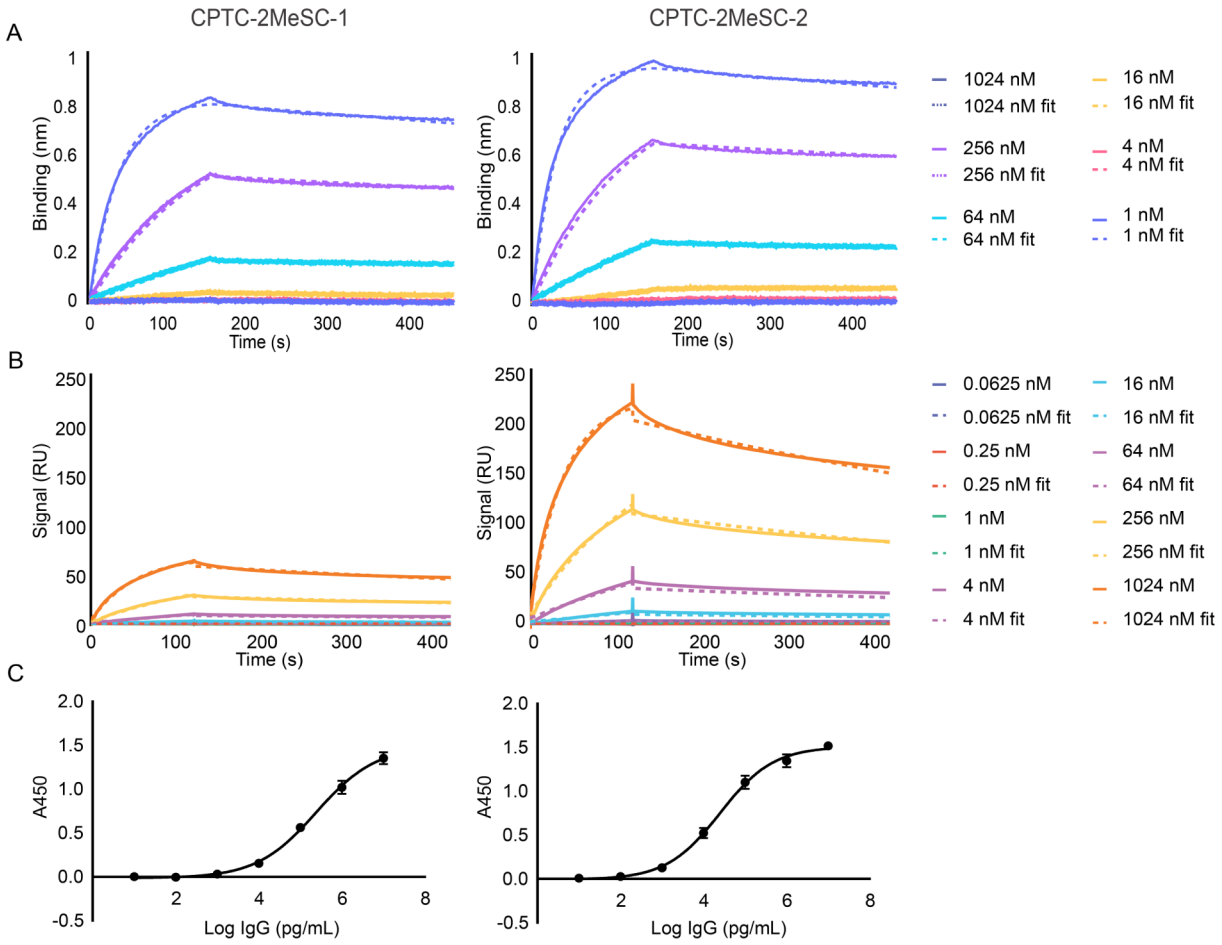


**Figure 3.** Measurements of affinity and kinetics toward ITA-Cys conjugated to BSA show stronger affinity of CPTC-2MeSC-2 than CPTC-2MeSC-1. (A) Biolayer interferometry (BLI) results of clones CPTC-2MeSC-1 (left) and CPTC-2MeSC-2 (right). CPTC-2MeSC clones were captured onto Protein G biosensors. BSA-conjugated ITA peptide was used as an analyte and was titrated at 1024, 256, 62, 16, 4, and 1.0 nM. Buffer only and biosensors immobilized without antibody were used as references for background subtraction. (B) Surface plasmon resonance (SPR) sensorgrams of CPTC-2MeSC-1 (left) and CPTC-2MeSC-2 (right). CPTC-2MeSC clones were captured onto a Series S Protein G biosensors chip. The BSA-conjugated ITA peptide was titrated over the antibody captured surface at 1024, 256, 64, 16, 4, 1.0, 0.25, and 0.0625 nM. Binding data were double-referenced. (C) Indirect ELISA of CPTC-2MeSC-1 (left) and CPTC-2MeSC-2 (right) against BSA-conjugated ITA peptide.

**Table 1. Binding affinity of CPTC-2MeSC-1 and CPTC-2MeSC-2 as measured by BLI, SPR, and Indirect ELISA[a]**

| | Bio-layer interferometry | | | Surface plasmon resonance | | | Indirect ELISA |
|---|---|---|---|---|---|---|---|
| | KD (M) | Ka (1/Ms) | Kd (1/s) | KD (M) | Ka (1/Ms) | Kd (1/s) | EC50 (ng/mL) |
| CPTC-2MeSC-1 | $1.2 \times 10^{-8}$ | $2.7 \times 10^{4}$ | $3.4 \times 10^{-4}$ | $4.8 \times 10^{-8}$ | $1.7 \times 10^{4}$ | $8.5 \times 10^{-4}$ | 243 |
| CPTC-2MeSC-2 | $8.9 \times 10^{-9}$ | $3.2 \times 10^{4}$ | $2.8 \times 10^{-4}$ | $4.1 \times 10^{-8}$ | $2.4 \times 10^{4}$ | $1.0 \times 10^{-3}$ | 25 |

[a]KD: equilibrium binding; Ka: association rate constant; Kd: stability of complex (rate of decay).

immunodetection, thus serving as binding competitors. The detection was carried out with the use of secondary antibodies conjugated to europium cryptate, followed by time-resolved fluorescence imaging. This allowed for a large dynamic range of detection and improved SNR. The results of the dot blot assay largely corroborated the data obtained with ELISA and plate-bound ITA/ITA-Cys. The BSA-ITA detection limit for clones 1G8, 2B4, and 3C2 reached 0.3 ng per spot (Figure 2D). Based on these data, two clones were identified: 2B4 and 3C2. Next, we used 2B4 and 3C2 in plate-bound cysteine assays employing various Michael electrophiles to test for specificity. Eight different compounds (plus ITA-Cys as a positive control) containing a reactive double bond with structural similarity to itaconate including mono-, di-, and tricarboxylic acids as well as various mono- and diesters have been reacted with a plate-bound cysteine as described above. The resulting plate-bound Michael adducts were then probed with 2B4 and 3C2 (Figure 2E). In line with the ELISA data above (Figure 2C), the ITA-Cys showed significantly higher signal than other analogs for both clones (ranging from 3.5 to 66.5-fold increase for 2B4 and from 14.9 to 65.5-fold increase for 3C2). Additionally, both clones displayed moderate immunoreactivity to DMI (absorbance: 0.80 ± 0.06 for 2B4, 0.17 ± 0.09 for 3C2). All other derivatives did not produce an immunoreactive signal that could be discerned from noise. In summary, antibody clones 2B4 and 3C2 were identified to have high immunoreactivity toward ITA-Cys and ITA-BSA while also displaying high selectivity for the nascent antigen ITA-Cys as well as DMI as compared to structurally similar cysteine-bound Michael adducts, including ester derivatives of


https://doi.org/10.1021/acsomega.4c08552
ACS Omega 2025, 10, 1110−1121

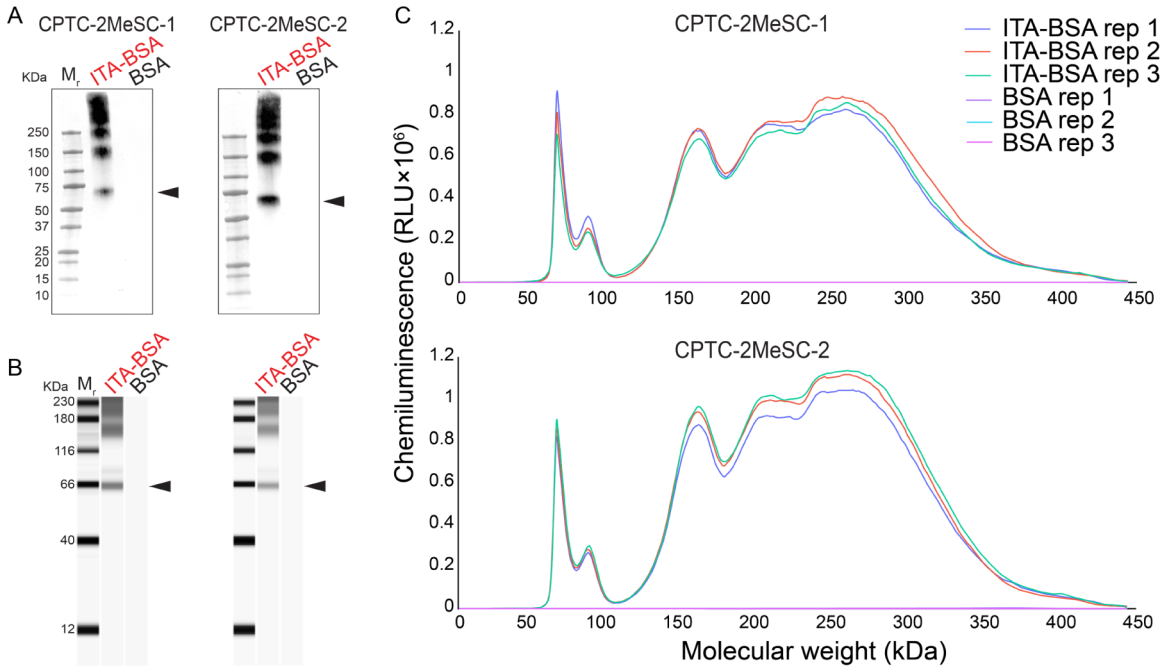


**Figure 4.** (A) Traditional Western blot using CPTC-2MeSC-1 (left) and CPTC-2MeSC-2 (right) as primary antibodies against ITA-BSA and BSA as negative control. (B) Simple Western blots of CPTC-2MeSC-1 (left) and CPTC-2MeSC-2 (right) as primary antibodies against the BSA-conjugated ITA peptide and BSA as negative control. Arrowheads point to a signal at 66 kDa representing ITA-Cys-conjugated BSA. (C) Electropherograms corresponding to the Simple Western virtual blots shown in panel B.

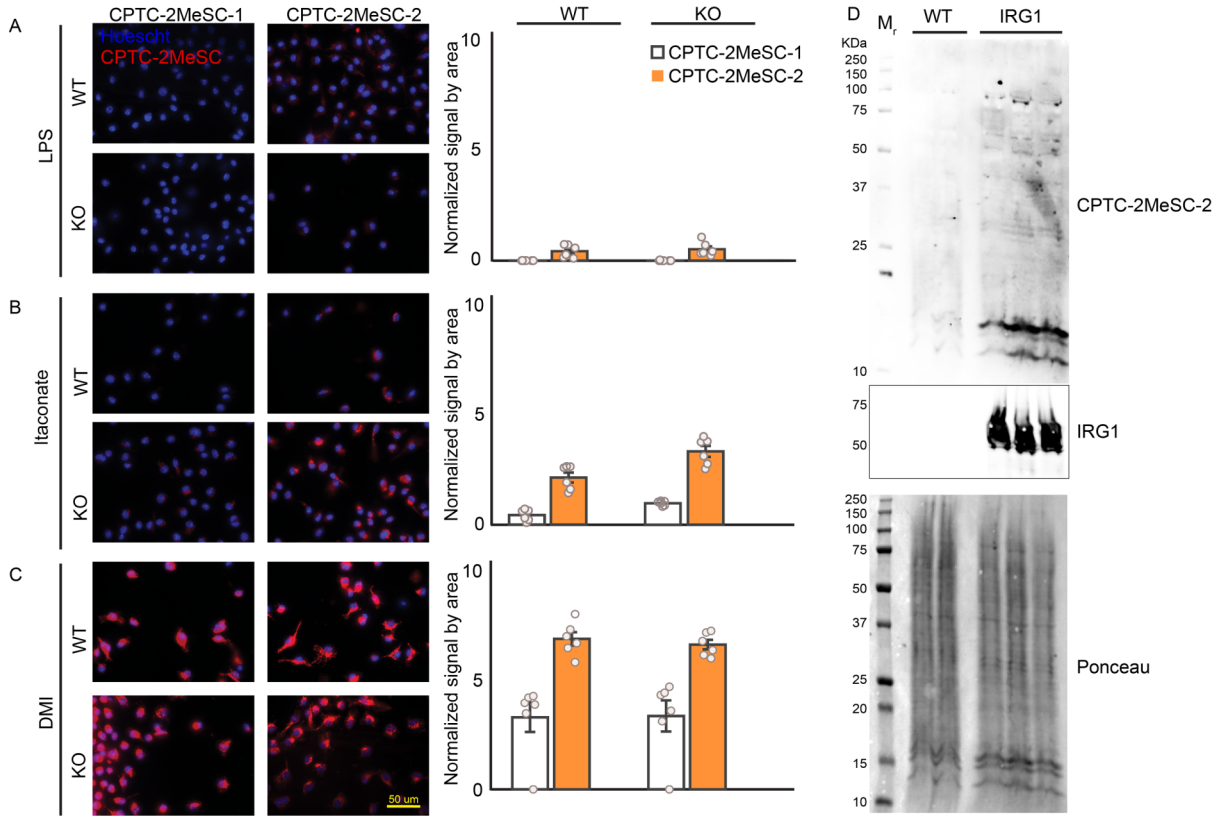


**Figure 5.** Experiments in vitro with antibodies CPTC-2MeSC-1 and CPTC-2MeSC-2. (A) LPS-treated wild type (WT) and IRG1-knockout (KO) bone marrow-derived macrophage (BMDM) representative images (left) and quantification by area normalized to Hoechst nuclear stain (right). (B) Itaconate-treated WT and KO BMDMs: images and quantification. (C) Dimethyl itaconate (DMI)-treated BMDMs: images and quantification. (D) Western blot images of IRG1-overexpressing HEK293 cell lysate probed with CPTC-2MeSC-2.

ITA such as methyl-ethyl- and octyl-itaconate. These two clones were then subcloned and purified via Protein A or Protein G Sepharose columns. Clone 2B4 became CPTC-2MeSC-1 and clone 3C2 became CPTC-2MeSC-2.



https://doi.org/10.1021/acsomega.4c08552
ACS Omega 2025, 10, 1110−1121

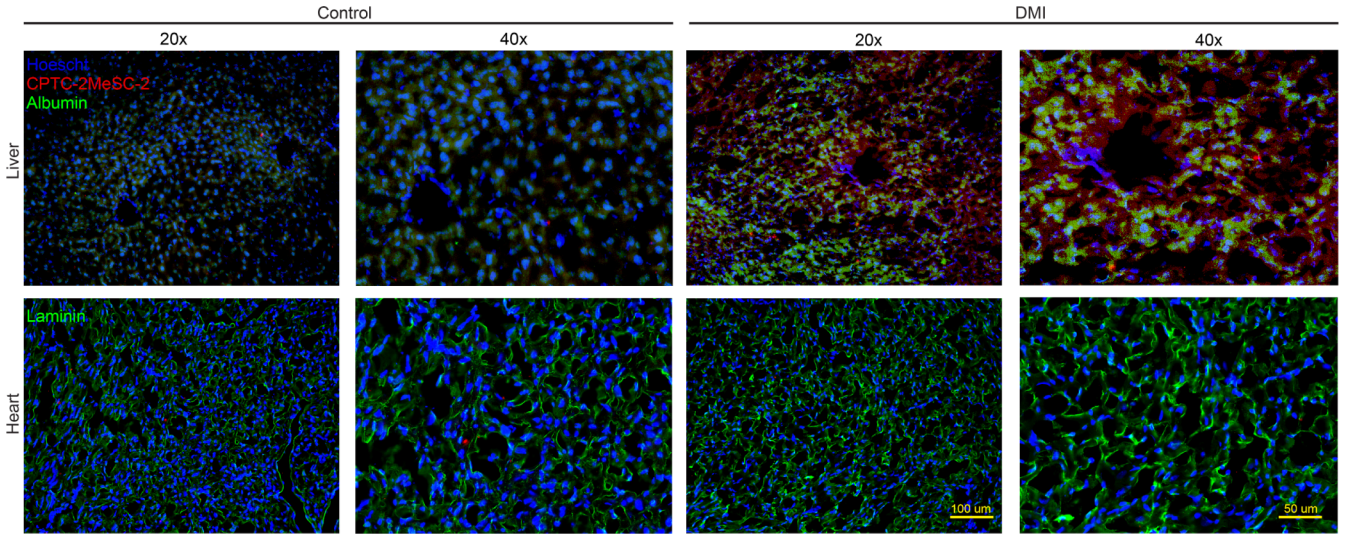


**Figure 6.** CPTC-2MeSC-2 binds to dimethyl itaconate in tissue from DMI-injected mice. DMI is detected in liver tissue (top) but not heart tissue (bottom). Blue is Hoescht nuclear stain, green is albumin in livers and laminin in hearts, and red is DMI conjugates as detected by CPTC-2MeSC-2. 40× magnification is shown to the right of each 20× magnification; scale bar = 100 $\mu$m in 20× and 50 $\mu$m in 40×.

Next, the binding affinity and kinetics of each respective antibody and BSA-conjugated ITA peptide were measured using biolayer interferometry and surface plasmon resonance. A summary of the binding affinity and kinetics parameters obtained from these tests is shown in Figure 3 and Table 1. CPTC-2MeSC-2 demonstrated stronger binding affinity to the BSA-conjugated ITA peptide than CPTC-2MeSC-1 in biolayer interferometry (KD = $8.9 \times 10^{-9}$ vs $1.2 \times 10^{-8}$ M). CPTC-2MeSC-2 also demonstrated stronger binding affinity than CPTC-2MeSC-1 in surface plasmon resonance (KD = $4.1 \times 10^{-8}$ vs $4.8 \times 10^{-8}$ M). Results from indirect ELISA testing showed a lower $EC_{50}$ value for CPTC-2MeSC-2 compared to that for CPTC-2MeSC-1 (25 vs 243 ng/mL) (Figure 3, Table 1).

Additional validation and usability of CPTC-2MeSC-1 and CPTC-2MeSC-2 for membrane-based assays were next carried out using two types of Western blotting. Using ITA-BSA as an antigen and BSA as a negative control, we performed a Western blot with manual processing (traditional) and with an automated system (ProteinSimple Simple Western). Both purified antibodies demonstrated binding to ITA-BSA (66 kDa band, Figure 4) in traditional Western blot and Simple Western, and no binding to BSA was observed. The detection of high-molecular-weight signals (>66 kDa) was also expected due to the presence of highly functionalized BSA and BSA aggregates both resulting from ITA-Cys conjugation. The virtual blot from Simple Western in Figure 4B shows the same pattern with a distinct signal at 66 kDa but no immunoreactivity toward BSA negative control. Figure 4C displays electropherograms from the Simple Western data in Figure 4B.

Successful validation of CPTC-2MeSC-1 and CPTC-2MeSC-2 specificity, selectivity, and affinity warranted testing of in vitro functionality. We tested antibody binding to both endogenous and exogenous itaconate in murine bone marrow-derived macrophages (BMDMs) from wild type (WT) and IRG1 knockout (KO) mice. Cells were treated with either (1) lipopolysaccharide (LPS) to induce inflammation and produce endogenous itaconate,[9,25,26] (2) itaconate, or (3) DMI for 24 h and then fixed and immunoprobed with CPTC-2MeSC-1 or CPTC-2MeSC-2. Images are shown in Figure 5A−C with the corresponding quantification based on the area to the right for each treatment condition. CPTC-2MeSC-2 outperformed CPTC-2MeSC-1 in all treatment conditions (by fold change: WT LPS 167.2 ± 45.6, KO LPS 77.1 ± 19.1; WT itaconate 5.0 ± 0.5, KO itaconate 3.4 ± 0.3; WT DMI 2.1 ± 0.1, and KO DMI 2.0 ± 0.1), and exogenous itaconate and DMI outperformed LPS-induced endogenous itaconate (by fold change relative to LPS: WT itaconate CPTC-2Me-SC-1 166.4 ± 40.9, CPTC-2Me-SC-2 5.0 ± 0.5; KO itaconate CPTC-2Me-SC-1 145.7 ± 6.4, CPTC-2Me-SC-2 6.4 ± 0.5; WT DMI CPTC-2Me-SC-1 1273.5 ± 258.5, CPTC-2Me-SC-2 15.9 ± 0.7; KO DMI CPTC-2Me-SC-1 494.0 ± 104.8, and CPTC-2Me-SC-2 12.6 ± 0.4). The LPS-induced itaconate showed no difference between the WT and IRG1 KO cells. Between exogenous itaconate species, both antibodies showed higher binding to DMI as compared to itaconate (by fold change: WT CPTC-2Me-SC-1 7.7 ± 1.6, CPTC-2Me-SC-2 3.2 ± 0.1; KO CPTC-2Me-SC-1 3.4 ± 0.7, and CPTC-2Me-SC-2 2.0 ± 0.1). Furthermore, to examine whether CPTC-2Me-SC-2 binds to the endogenous itaconate conjugates produced by continuous exposure to intracellular itaconate, we overexpressed human IRG1 protein in HEK293 cells. The lysates from IRG1 null (i.e., wild-type) and IRG1-overexpressed HEK293 cells were then probed with CPTC-2Me-SC-2 in a Western blotting experiment (Figure 5D). The results show strong CPTC-2Me-SC-2 immunoreactivity in IRG1-overexpressing lysates for low molecular weight (∼10−15 kDa) and moderate immunoreactivity for mid-molecular-weight proteins (∼75−100 kDa). In contrast, IRG1 null HEK293 cell lysates did not exhibit specific immunoreactivity to CPTC-2Me-SC-2.

Finally, we demonstrated that CPTC-2Me-SC-2 can be successfully used in in vivo applications. Wild-type C57BL/6J mice were injected with 500 mg/kg DMI intraperitoneally and euthanized 2 h postinjection. Livers and hearts were probed with CPTC-2MeSC-2 and examined by immunofluorescence (Figure 6). To identify intratissue localization of the DMI signal, livers were also probed with antialbumin antibodies known to identify hepatocytes,[27−30] while hearts were probed with antilaminin antibodies to outline cardiomyocytes.[31−34] As expected,[35−37] DMI accumulation in the liver produced an


https://doi.org/10.1021/acsomega.4c08552
ACS Omega 2025, 10, 1110−1121

intense, widespread signal that was detected within albumin-positive hepatocytes. We did not observe DMI accumulation in heart tissue.

## DISCUSSION

Itaconate has proven to be a metabolite of great potential for wide-ranging therapies based on its immunomodulatory properties, with steadily increasing interest in the past 50 years. In that time, itaconate publications have risen from 2 in 1974 to 16 in 2004 and to 58 in 2014, reaching 216 in 2023 (via PubMed). Given the momentum in the field, it follows that there is a demand for sensitive methods to detect itaconate. In this work, we have developed an antibody, CPTC-2MeSC-2, for use in studying itaconate and its derivatives. The applications for this antibody are numerous, ranging from locating itaconate species intracellularly in vivo (which we demonstrate in this work as proof of concept) to furthering mechanistic understanding by studying itaconate-modified proteins (out of this work's scope but impactful for the field).

CPTC-2MeSC-2 demonstrates nanomolar affinity toward its target, ITA-Cys, with a KD value of $8.9 \times 10^{-9}$ M by biolayer interferometry and an EC50 value of 25 ng/mL by indirect ELISA. Importantly, the antibody does not bind to Michael adducts of structurally similar metabolites such as cis-aconitic acid, fumaric acid, and citraconic acid (Figure 2). We have shown that CPTC-2MeSC-2 demonstrates specificity toward itaconate, its derivatives, and conjugates. We developed an ELISA-style plate assay that allows testing of different Michael adducts immobilized on a plate surface. To the best of our knowledge, this is the first time an antimetabolite antibody has gone through rigorous cross-testing of this type.

In vitro, CPTC-2MeSC-1 and CPTC-2MeSC-2 successfully identified exogenous itaconate and dimethyl itaconate. Endogenously produced itaconate resulted in a lower signal, likely because itaconate is well-known to be secreted by macrophages into the extracellular environment and thus may not be retained intracellularly.[7,38] Another possibility is that the low signal may be reflective of a minimal response to LPS treatment. It is possible that a higher concentration of LPS would result in higher intracellular itaconate production and an improved signal. Though we did not test different LPS concentrations because this is beyond the scope of this article, such an experiment could be proven technically challenging due to reduced cellular viability in response to high levels of LPS. Instead, the binding of CPTC-2MeSC-2 to the endogenous itaconate conjugates was tested in IRG1-over-expressing HEK293 cells. HEK293 null cells neither express endogenous IRG1 nor produce itaconate. The IRG1 over-expression in these cells thus circumvented the search for optimal conditions in macrophages and allowed for straightforward testing of the CPTC-2MeSC-2 immunoreactivity. Intriguingly, the CPTC-2MeSC-2 signal in IRG1-overexpressing lysates was mostly restricted to 10−15 kDa proteins, suggesting the likelihood of post-translational histone modifications. Itaconate-mediated lysine acylation of histones (termed "itaconation") has been previously reported.[39] However, histone cysteine itaconation has never been previously detected using antibody-based methods. Investigating the susceptibility of histones to cysteine itaconation and the resultant biological function of such a modification is a warranted endeavor of future research.

We have demonstrated that with CPTC-2MeSC-2, we are able to identify hepatic localization of intraperitoneally injected dimethyl itaconate. Dimethyl itaconate and itaconate are known to have in vivo action in the liver,[26,40,41] but this is the first report of which we are aware that shows intratissue accumulation of either molecule. We were also interested in potential uptake of DMI by the heart, given that previous studies have demonstrated that systemic treatment with DMI produced various broad beneficial cardiovascular effects.[7,42−44] Interestingly, we did not see accumulation of DMI in heart tissue upon intraperitoneal injection, indicating that its previously reported therapeutic actions likely stem from its broad systemic effects rather than local effects in cardiac muscle. This finding is intriguing and may inform the development of itaconate-based therapies for cardiac indications.[44,45]

## METHODS

**General.** All chemicals of the highest grade were purchased from Thermo Fisher or Millipore Sigma unless otherwise noted. All organic solvents were of HPLC grade and were purchased from Millipore Sigma. Mice were purchased from Jackson Laboratories and were strain C57BL/6J males unless specified otherwise.

*ITA-Cys Hydrochloride [3-((4-Ethoxy-2-(ethoxycarbonyl)-4-oxobutyl)thio)-1-methoxy-1-oxopropan-2-aminium chloride], Figure 2a.* *N*-(*tert*-butoxycarbonyl)-L-cysteine methyl ester (2, Millipore Sigma 467154) at 10 mmol (2.35 g) was mixed with 11 mmol (2.05 g) of diethyl itaconate (1, TCI America I0204) under a nitrogen atmosphere and reacted with gentle stirring under nitrogen for 24 h at room temperature. The resulting Michael adduct 3 was then mixed with 10 mL of 4 M hydrogen chloride solution in dioxane (Millipore Sigma 345547) at 0 °C for 30 min with stirring. The mixture was brought to room temperature and evaporated under the stream of nitrogen gas followed by drying under high vacuum (0.03 mTor) for 24 h at room temperature. Next, the residue was dissolved in 30 mL diethyl ether and incubated at −80 °C for 24 h. The white precipitate was formed that was separated by filtration and dried under vacuum, resulting in 3.57 g (4, 100%) of 3-((4-ethoxy-2-(ethoxycarbonyl)-4-oxobutyl)thio)-1-methoxy-1-oxopropan-2-aminium chloride.

$^1$H NMR (500 MHz, $D_2O$) $\delta$ 4.43 (dd, $J$ = 7.1, 4.6 Hz, 1H), 4.20 (dq, $J$ = 24.3, 7.1 Hz, 4H), 3.88 (s, 1H), 3.25 (ddd, $J$ = 15.0, 4.6, 1.5 Hz, 1H), 3.21−3.10 (m, 2H), 2.99−2.89 (m, 1H), 2.86−2.74 (m, 2H), 1.26 (dt, $J$ = 10.9, 7.2 Hz, 6H). 13C NMR (126 MHz, $D_2O$) $\delta$: 175.28, 173.82, 173.80, 169.06, 169.03, 62.48, 53.81, 53.79, 52.18, 41.62, 35.12, 32.91, 31.42, 13.24. HRMS: expected (neutral) $m/z$ 321.1246; measured (neutral) $m/z$ 321.1254; expected ($MH^+$) $m/z$ 322.1324; measured ($MH^+$) $m/z$ 322.1327.

*ITA-Cys Squarate 6 [Diethyl 2-(((3-Methoxy-2-((2-methoxy-3,4-dioxocyclobut-1-en-1-yl)amino)-3-oxopropyl)thio)methyl)succinate].* 100 mg portion (0.28 mmol) of **4** was mixed with 65 $\mu$L of sodium methoxide (25% in methanol, 16.2 mg, 0.3 mmol, Millipore Sigma 156256) in 500 $\mu$L of dry methanol, and the solution was evaporated to dryness under a stream of nitrogen gas and then under high vacuum. The resulting residue was taken in 0.5 mL of carbon tetrachloride and filtered using a nylon 0.2 $\mu$m spin filter. This solution was then added to 35.5 mg (0.25 mmol) of dimethyl squarate **5** (Millipore, Sigma 377406). The mixture was shaken at room temperature for 18 h. The solvent was then evaporated under a


https://doi.org/10.1021/acsomega.4c08552
ACS Omega 2025, 10, 1110−1121

stream of nitrogen gas and under high vacuum, resulting in 120 mg (99%) of **6** as a yellow oil.

*ITA-Cys KLH and BSA Conjugate.* 50 mg of **6** was mixed with 10 mg of hemocyanin from*Megathura crenulata*(keyhole limpet, Millipore Sigma H7017) or with 10 mg of bovine serum albumin (Millipore Sigma A9647) in 0.2 mL of 0.1 M sodium carbonate solution at pH 11. The mixtures were gently agitated by end-overrotation at 4 °C for 24 h after which they were transferred into a dialysis cassette (MWCO 20 kDa) and dialyzed at 4 °C against five 2 L changes (6 h each) of 10 mM phosphate buffered saline PBS). The completion of the hydrolysis reaction (full hydrolysis of methyl and ethyl esters) was ensured by initially monitoring the reactions in $D_2O$ solutions while registering liberation of the free methanol and ethanol by NMR. The resulting conjugates were sterile-filtered through a 0.2 $\mu$m membrane, and the protein content was determined by BCA protein assay (Thermo Fisher 23227).

**ELISA for Antibody Selectivity.** Enzyme-linked immunosorbent assays (ELISAs) were run in clear 96-well maleic anhydride plates (Pierce; ThermoFisher cat. 15100). Wells were treated with 50 $\mu$g/mL (+)-*S*-trityl-L-cysteine (Millipore Sigma cat. 164739) in a bicarbonate buffer (pH 9) and sealed overnight at 37 °C. Positive control wells were treated with 50 $\mu$g/mL ITA-Cys instead of (+)-*S*-trityl-L-cysteine. Wells were washed with PBS and ethanol and dried at 50 °C. Protecting groups were removed from cysteine with 3 mM triethyl silane in trifluoroacetic acid for 30 min under nitrogen gas. Wells were washed with cold methanol three times and then with double distilled water three times. Antigen (various Michael acceptors as depicted in Figure 2E) was added to the plate at 0.3 mM in water or water/DMSO as necessary for solubility. The plate was sealed and incubated overnight at 37 °C. Wells were washed with PBS and blocked with 5% milk in TBST for 1 h. Wells were washed with PBS, and the primary antibody was added at 1:100 dilution in 5% milk in TBST, sealed, and incubated overnight at 4 °C. Wells were washed with PBS, and the rabbit antimouse superclonal IgG secondary antibody HRP-conjugated (Thermo Fisher cat. A27025) was added at 1:5000 in 1% BSA in TBST for 1 h at room temperature. Wells were washed with PBS, and tertiary antibody, goat antirabbit HRP-conjugated (Thermo Fisher cat. A27036) was added at 1:5000 dilution in 1% BSA/TBST for 1 h while being protected from light. Wells were washed with PBS and treated with 3,3′, 5,5-tetramethylbenzidine chromogen solution (Sigma-Aldrich cat. T4444) for about 10 min; the reaction was stopped with 2 M HCl and plate was read at 450 nm on a SpectraMax i3 plate reader.

**Macrophage Differentiation.** Bone marrow-derived macrophages were acquired by isolating bone marrow cells from a wild-type mouse (C57BL/6J, Jackson Laboratories) and an IRG1 knockout mouse (C57BL/6NJ-Acod1$^{em1(IMPC)J}$/J, Jackson Laboratories). Cells were differentiated into macrophages by treatment with mouse macrophage colony-stimulating factor (mCSF; Miltenyi Biotec cat. 130-101-706) at 40 ng/mL in DMEM media (Sigma-Aldrich cat. D6546) with 20% fetal bovine serum and 1% antibiotic−antimycotic for 6 days in tissue culture-treated dishes at 37 °C and 5% humidity. Cells were monitored for differentiation based on their appearance under a light microscope.

**In Vitro Immunostaining.** Differentiated macrophages were plated at 200k/well in 18-well IBIDI chamber slides with ibiTreat surface (IBIDI cat. 81816) in complete DMEM. When cells had adhered, they were treated with lipopolysaccharide (Millipore Sigma cat. L2630) at 100 ng/mL, itaconate (Millipore Sigma cat. 93598, pH-adjusted to 7.2) at 1 mM, or dimethyl itaconate (Millipore Sigma cat. 109533) at 0.125 mM for 24 h at 37 °C. Cells were then fixed by washing in cold PBS and then treated with 4% paraformaldehyde in PBS for 10 min. Wells were washed with TBST and then blocked with 0.3% Triton X100 (Fisher Scientific cat. MRKBP1512OL) in Aqua Block Reagent (Millipore Sigma cat. 558300) for 30 min. The primary antibody was then added at a 1:50 dilution in 0.3% Triton in an Aqua Block. Slides were sealed and incubated at 4 °C overnight. Secondary antibodies were added at 1:200 dilution in 2% BSA in TBST for 1 h. Secondary antibodies corresponded to the isotype of the primary antibody: goat antimouse IgG1 Alexa Fluor 647 (ThermoFisher cat. A-21240), goat antimouse IgG2a Alexa Fluor 647 (ThermoFisher cat. A-21241), goat antimouse IgG2b Alexa Fluor 647 (ThermoFisher cat. A-21242), and donkey antirabbit IgG (H+L) Alexa Fluor 647 (ThermoFisher cat. A-31573). Hoechst nuclear stain (ThermoFisher cat. 62249) was added to wells at a dilution of 1:1000 in PBS for 20 min at room temperature protected from light. Wells were washed with PBS before imaging. Imaging was done on a Keyence BZ-X710 microscope with a 620/660 filter.

**IRG1 Overexpression in HEK293 Cells.** A puromycin-resistant stable HEK293 cell line overexpressing human IRG1 was produced as previously described by us.[46] Briefly, HEK293 cells (ATCC cat. CRL-1573) were cultured in high-glucose DMEM supplemented with 10% FBS and 1% penicillin/streptomycin. Transfection was performed using a human ACOD1 (IRG1) plasmid under a CMV promoter and puromycin resistance from Vector Builder, with X-tremeGENE HP DNA Transfection Reagent (Millipore Sigma cat. 6366244001). The cells were treated at a 3:1 ratio of transfection reagent to DNA for 48 h with a plasmid concentration at 1 $\mu$g per million cells. After 48 h of transfection, puromycin was added to the cells at 1.5 $\mu$g/mL to maintain the expression of IRG1 in proliferating cells. The puromycin concentration was determined by the kill curve in wild-type HEK293 cells; 1.5 $\mu$g/mL was determined to be the lowest concentration that was cytotoxic in wild type cells. The overexpression of IRG1 was then confirmed through Western blotting experiments in cell lysates with an antihuman IRG1 rabbit mAb (Cell Signaling Technology cat. 77510). Wild-type and IRG1 HEK293 cells were then plated in six-well plates and cultured at a density of $2 \times 10^6$/mL for 24 h, after which the cells were lysed and subjected to Western blot immunoprobing as described below using the CPTC-2MeSC-2 antibody at 10 $\mu$g/mL as a primary antibody and HRP-conjugated goat antimouse IgG2b as polyclonal secondary antibody (Thermo Fisher cat. M32407) at 1 $\mu$g/mL.

**Dot Blot.** For direct blotting experiments, a nitrocellulose membrane was used. 2 $\mu$L of the ITA-Cys BSA conjugate was spotted on the membrane at different concentrations per spot (30, 3, 0.3, and 0.03 ng) and dried at 37 °C for 1 h. The membrane was then blocked with 5% milk in TBS for 1 h at room temperature. In some experiments, the immunodetection was performed in the presence of a competitor: either itaconate sodium (100 mM) or ITA-Cys (100 mM), with primary antibody diluted at 1:500 (10 $\mu$g/mL) in Aqua Block containing 0.1% Tween 20. The membrane was incubated at 4 °C overnight, after which it was washed in TBST four times with shaking. The secondary antibody was trFluor europium goat antimouse IgG (AAT Bioquest cat. 16755) that was


https://doi.org/10.1021/acsomega.4c08552
ACS Omega 2025, 10, 1110−1121

diluted at 1 μg/mL in Aqua Block containing 0.1% Tween 20. The incubation proceeded for 1 h at room temperature. After washing with TBST four times and with distilled water 2 times, the membrane was dried at 37 °C for 1 h. Dried membranes were imaged using a time-resolved fluorescence module on a SpectraMax i3 imager and analyzed using Molecular Devices TRF Western blot software.

**In Vivo Immunohistochemistry.** C57BL/6J mice (Jackson lab) were injected with 500 mg/kg of DMI in DMSO intraperitoneally. Two hours later, mice were euthanized with isofluorane. Mice were perfused in the following order: PBS, 4% PFA in PBS, and 5% OCT in PBS. Each solution perfused for 3 min. Hearts and livers were removed and placed in OCT and frozen at −80 °C. Sections were sliced at 10 μm-thick and adhered to glass slides with OCT. Slides were kept at −20 °C until ready for use, at which point they were dried and washed with PBS. Tissues were permeabilized with 0.5% Triton (ThermoFisher cat. BP151-100) in Seablock (ThermoFisher cat #37527) for 30 min at room temperature and then blocked at room temperature for 30 min with Rodent Block M (Biocare Medical cat. RBM961). The primary antibody was then added at 1:50 dilution in 0.5% Triton in Seablock and incubated overnight at 4 °C (antialbumin from Santa Cruz Biotechnology cat. sc-271605; anti-laminin Sigma-Aldrich cat. L9393). CPTC-2MeSC was preincubated with the secondary antibody also at 1:50 dilution (ChromoTek Nanosecondary alpaca antimouse IgG2b CoraLite Plus 647, Proteintech cat. smsG2bCL647-1) for 1 h at room temperature before incubation to reduce nonspecific binding by the secondary species to other mouse proteins present in the tissues. Slides were washed and then secondary antibodies (donkey anti-Rabbit IgG Alexa Fluor Plus 488 (ThermoFisher cat. A32790) and goat anti-Ms IgG1 Alex Fluor 488 (ThermoFisher cat. A21121)) were added at 1:200 in 0.5% Triton in Seablock for 1 h at room temperature. Hoechst nuclear stain (ThermoFisher cat. 62249) was added to slides at a dilution of 1:1000 in PBS for 10 min at room temperature protected from light. Slides were washed and imaged on a Keyence BZ-X710 microscope.

**Western Blot.** Western immunoassays were performed by using traditional immunoblotting techniques. ITA-BSA (positive control) and BSA (negative control) were loaded on a Criterion TGX Precast gel (BioRad cat. 6571024). Samples were conducted at a concentration of 10 μg/mL under reducing conditions (200 ng total protein). Transfer of protein from the precast gel to a PVDF membrane (Bio-Rad cat. 1704157) was performed by Bio-Rad Turbo-Blot at a "high MW" setting for 10 min. Blocking of the membrane was performed using Bio-Rad Blotting grade Blocker at 5% in 1× PBS−0.5% Tween-20. Primary antibodies (1 mg/mL) were diluted in 1× PBS−0.5% Tween-20 to a dilution of 1:5000 at a total volume of 25 mL. Washing of the membrane was conducted using 1× PBS−0.5% Tween-20 three times. The secondary HRP-linked mouse specific antibody (Jackson ImmunoResearch cat. 115-035-146) was diluted at 1:5000 in 1× PBS−0.5% Tween-20 at a volume of 25 mL. Immunodetection was performed using Clarity Western ECL Substrate (BioRad cat. 1705061), following the manufacturer's protocol. Development of the immunoblot was captured by using the Bio-Rad ChemiDocMP imaging system.

**Simple Western.** The Simple Western (Jess, ProteinSimple, USA) system was used to detect the binding of the primary antibody to ITA-BSA (positive control) and BSA (negative control). Samples were run using the 12−230 kDa separation module (Bio-Techne, ProteinSimple cat. SM-W004) and detected with an Anti-Mouse Detection Module (Bio-Techne, ProteinSimple cat. DM-002). Samples had a concentration of 0.2 mg/mL, and the antibodies were diluted to 1:500.

**Surface Plasmon Resonance.** The affinity and binding kinetics of mouse antibodies CPTC-2MeSC-1 and CPTC-2MeSC-2 and the corresponding ITA-BSA were measured using surface plasmon resonance. All binding studies were performed using a Cytiva Biacore T200 instrument. The procedure is described in SOP M-140 on the antibodies.cancer.gov portal. All assays were performed in freshly prepared running buffer containing 10 mM HEPES, 150 mM NaCl, 3 mM EDTA, and 0.05% (v/v) Surfactant P20 at 25 °C. Mouse antibodies were captured onto a Series S Protein G biosensor chip (Cytiva cat. 29179315) by injecting 1−2 μg/mL of the antibody diluted in a running buffer for 60 s at a 10 μL/min flow rate on active flow cells. 4-fold dilutions of the ITA-BSA (0.0625−1024 nM) were injected using a contact time of 120 s at 30 μL/min. The dissociation of the ITA-BSA from the antibody was monitored for 300 s. At the end of each cycle, the surface was regenerated for 30 s at 30 μL/min using 10 mM glycine (pH 1.5). The data were analyzed using Biacore T200 Evaluation Software, version 3.2. All binding data were double-referenced and analyzed globally using a 1:1 fitting model.

**Bio-Layer Interferometry.** The binding affinity and kinetics of mouse antibodies CPTC-2MeSC-1 and CPTC-2MeSC-2 and the corresponding BSA-conjugated ITA peptide were measured using biolayer interferometry. All binding studies were performed using the Sartorius Fortebio Octet Red 96e system (Sartorius, CA, USA). The procedure is described in SOP M-141 on the antibodies.cancer.gov portal. Individual Octet Protein G biosensors (Sartorius cat. 18-5082) were hydrated in $H_2O$ for 10 min. Respective mouse antibodies were loaded onto the Protein G biosensors for 300 s. After equilibration with a 1× kinetics buffer for 2 min and a baseline measurement of 2 min, the sensors were transferred into ITA-BSA, 0.25−1024 nM, to evaluate binding. Association was measured for 2.5 min, and dissociation was measured for 5 min. The data were analyzed using ForteBio Data Analysis HT 11.1 software (ForteBio, CA, USA). All binding data were double-referenced and analyzed globally using a 1:1 fitting model.

**Indirect ELISA.** EC50 values were determined for antibodies CPTC-2MeSC-1 and CPTC-2MeSC-2 and BSA-conjugated ITA using indirect ELISA following SOP M-102. Briefly, BSA-conjugated ITA was coated in triplicate on medium-binding 96-well polystyrene microtiter plates (Corning cat. 9017). The fourth row of wells are not coated with antigen but with only the coating buffer, and this is the blank wells. This is used for blank subtracted data. Wells were incubated with blocking buffer (PBS, 0.05% Tween-20, 0.5% milk) and incubated for 1 h. Wells were washed 3× with PBS-T. The antibody at respective dilutions was added to wells in triplicate and incubated for 1 h at 37 °C while shaking. After washing three times with PBS-T, wells were incubated with HRP-conjugated antimouse antibodies for 1 h at 37 °C. Wells were washed three times with PBS-T and were developed using the TMB substrate. Reactions were stopped using 0.18 N sulfuric acid. Absorbance at 450 nm was measured immediately by using a Tecan spark microplate reader. Data were fit using a four parameter logistic (4PL) regression model to obtain EC50


https://doi.org/10.1021/acsomega.4c08552
ACS Omega 2025, 10, 1110−1121

values (https://www.myassays.com/four-parameter-logistic-regression.html).

**Immunization and Hybridoma Selection.** OriGene Technologies Inc. performed the immunizations of mice for antibody generation. Female BALB/c mice (12 weeks old) were injected subcutaneously with 80−160 μg of ITA-KLH emulsified in complete Freund's adjuvant. Two additional injections of 40−80 μg of antigen emulsified in incomplete Freund's adjuvant were followed at biweekly intervals starting 4 weeks after the first immunization. Ten days after the second boost, the serum antibody titer was tested using ELISA. Two weeks after the second boost, the mice were given a final booster injection intraperitoneally with 40−80 μg of protein. Three days after the last injection, spleen cells from the immunized mice were fused with myeloma Sp2/0 cells.[47]

**Hybridoma Production and Antibody Purification.** OriGene Technologies Inc. isolated the hybridomas, subcloned the clones of interest, and performed the final antibody purification. Hybridoma was passaged and expanded when cells were in the exponential phase of their growth cycle. The supernatant was harvested when the desired volume and viability were reached. Culture medium was harvested by spinning the supernatant at 8000 rpm for 15 min at 4 °C and then filtered using 0.45 μm filtration membranes. Protein A or Protein G sepharose 4FF beads (Smart-Lifesciences; Protein A beads [Cat: SA02301L], rProtein G beads, Cat: SA02001L) were equilibrated with at least 3 column volumes of 1× PBS. The filtered supernatant and Protein A or Protein G sepharose 4FF beads were mixed and bound for 4 h at 4 °C. The bound antibodies were eluted using 0.1 M glycine (pH 2.8). Fractions were collected. The eluted antibodies were neutralized using 1 M Tris-HCl (pH 9.0). Antibodies were dialyzed against two or three changes of 1× PBS over 24−48 h.

## ■ ASSOCIATED CONTENT

### Data Availability Statement

ITA-Cys, ITA-BSA, and ITA-KLH can be obtained from the authors upon reasonable request. CPTC-2MeSC-1 and CPTC-2MeSC-2 mAb can be obtained from the Developmental Studies Hybridoma Bank at dshb.biology.uiowa.edu. Characterization data related to these monoclonal antibodies can be found at antibodies.cancer.gov.

## ■ AUTHOR INFORMATION


### Corresponding Author

**Andrei Maiseyeu** − *Department of Medicine, School of Medicine, Case Western Reserve University, Cardiovascular Research Institute, Cleveland 44106-7078, United States; Department of Biomedical Engineering, Case Western Reserve University, Cleveland 44106, United States;* orcid.org/0000-0001-8830-1809; Email: axm1079@case.edu

### Authors

**Lauren Switala** − *Department of Medicine, School of Medicine, Case Western Reserve University, Cardiovascular Research Institute, Cleveland 44106-7078, United States; Department of Biomedical Engineering, Case Western Reserve University, Cleveland 44106, United States;* orcid.org/0000-0002-8121-2181

**Lin Di** − *Department of Medicine, School of Medicine, Case Western Reserve University, Cardiovascular Research Institute, Cleveland 44106-7078, United States; Department of Biomedical Engineering, Case Western Reserve University, Cleveland 44106, United States;* orcid.org/0000-0001-6123-0422

**Simona Colantonio** − *Cancer Research Technology Program, Antibody Characterization Lab, Frederick National Laboratory for Cancer Research, Frederick, Maryland 21701, United States*

**Bindu Lakshman** − *Cancer Research Technology Program, Antibody Characterization Lab, Frederick National Laboratory for Cancer Research, Frederick, Maryland 21701, United States*

**Tessa W. Caceres** − *Cancer Research Technology Program, Antibody Characterization Lab, Frederick National Laboratory for Cancer Research, Frederick, Maryland 21701, United States*

**Joshua J. Reading** − *Cancer Research Technology Program, Antibody Characterization Lab, Frederick National Laboratory for Cancer Research, Frederick, Maryland 21701, United States*

**Sandra S. Garcia-Buntley** − *Cancer Research Technology Program, Antibody Characterization Lab, Frederick National Laboratory for Cancer Research, Frederick, Maryland 21701, United States*

Complete contact information is available at: https://pubs.acs.org/10.1021/acsomega.4c08552


### Author Contributions

Conceptualization: A.M. Data curation: L.S., L.D., and A.M. Formal analysis: L.S., L.D., S.C., B.L., T.W.C., J.J.R., S.S.G.-B., and A.M. Funding acquisition: A.M. Investigation: L.S., L.D., S.C., B.L., T.W.C., J.J.R., S.S.G.-B., and A.M. Methodology: L.S., L.D., and A.M. Project administration: A.M. Supervision: A.M. Validation: A.M. Visualization: L.S., L.D., and A.M. Writing − original draft: L.S., L.D., and A.M. Writing − review and editing: L.S., L.D., and A.M.

### Notes

All procedures involving animals were in compliance with the ethical principles established by the National Institutes of Health Guide for the Care and Use of Laboratory Animals (NIH Publications No. 8523, revised 2011).

The authors declare no competing financial interest.

## ■ ACKNOWLEDGMENTS

This work was supported by the National Heart, Lung, and Blood Institute (NHLBI), grants HL130516, HL155450, and the National Institute of Environmental Health Sciences ES033670 to A.M. This work was supported in part by the National Cancer Institute's Clinical Proteomics Tumor Analysis Consortium (CPTAC)'s Antibody Characterization Program (antibodies.cancer.gov).

## ■ REFERENCES

(1) Li, R.; Zhang, P.; Wang, Y.; Tao, K. Itaconate: A metabolite regulates inflammation response and oxidative stress. *Oxid. Med. Cell. Longev.* **2020**, *2020*, 5404780.

(2) O'Neill, L. A. J.; Artyomov, M. N. Itaconate: the poster child of metabolic reprogramming in macrophage function. *Nat. Rev. Immunol.* **2019**, *19*, 273−281.

(3) Baup, S. Ueber eine neue Pyrogen-Citronensäure, und über Benennung der Pyrogen-Säuren überhaupt. *Ann. Pharm.* **1836**, *19* (1), 29−38.

(4) Michelucci, A.; Cordes, T.; Ghelfi, J.; Pailot, A.; Reiling, N.; Goldmann, O.; et al. Immune-responsive gene 1 protein links

metabolism to immunity by catalyzing itaconic acid production. *Proc. Natl. Acad. Sci. U. S. A.* **2013**, *110*, 7820−7825.
(5) McFadden, B. A.; Purohit, S. Itaconate, an isocitrate lyase-directed inhibitor in Pseudomonas indigofera. *J. Bacteriol.* **1977**, *131*, 136−144.
(6) Shin, J.-H.; Yang, J.-Y.; Jeon, B.-Y.; Yoon, Y. J.; Cho, S.-N.; Kang, Y.-H.; et al. (1)H NMR-based metabolomic profiling in mice infected with Mycobacterium tuberculosis. *J. Proteome Res.* **2011**, *10*, 2238−2247.
(7) Lampropoulou, V.; Sergushichev, A.; Bambouskova, M.; Nair, S.; Vincent, E. E.; Loginicheva, E.; et al. Itaconate Links Inhibition of Succinate Dehydrogenase with Macrophage Metabolic Remodeling and Regulation of Inflammation. *Cell Metab.* **2016**, *24*, 158−166.
(8) Mills, E. L.; Ryan, D. G.; Prag, H. A.; Dikovskaya, D.; Menon, D.; Zaslona, Z.; et al. Itaconate is an anti-inflammatory metabolite that activates Nrf2 via alkylation of KEAP1. *Nature* **2018**, *556*, 113−117.
(9) Peace, C. G.; O'Neill, L. A. The role of itaconate in host defense and inflammation. *J. Clin. Invest.* **2022**, *132*, 132.
(10) Zecchini, V.; Paupe, V.; Herranz-Montoya, I.; Janssen, J.; Wortel, I. M. N.; Morris, J. L.; et al. Fumarate induces vesicular release of mtDNA to drive innate immunity. *Nature* **2023**, *615*, 499−506.
(11) Mills, E. L.; Kelly, B.; Logan, A.; Costa, A. S. H.; Varma, M.; Bryant, C. E.; Tourlomousis, P.; Däbritz, J. H. M.; Gottlieb, E.; Latorre, I.; Corr, S. C.; et al. Succinate dehydrogenase supports metabolic repurposing of mitochondria to drive inflammatory macrophages. *Cell* **2016**, *167* (2), 457−470.e13.
(12) Hayes, J. D.; Dinkova-Kostova, A. T. The Nrf2 regulatory network provides an interface between redox and intermediary metabolism. *Trends Biochem. Sci.* **2014**, *39*, 199−218.
(13) Bambouskova, M.; Gorvel, L.; Lampropoulou, V.; Sergushichev, A.; Loginicheva, E.; Johnson, K.; et al. Electrophilic properties of itaconate and derivatives regulate the IκBζ-ATF3 inflammatory axis. *Nature* **2018**, *556*, 501−504.
(14) Swain, A.; Bambouskova, M.; Kim, H.; Andhey, P. S.; Duncan, D.; Auclair, K.; et al. Comparative evaluation of itaconate and its derivatives reveals divergent inflammasome and type I interferon regulation in macrophages. *Nat. Metab.* **2020**, *2*, 594−602.
(15) Nakkala, J. R.; Yao, Y.; Zhai, Z.; Duan, Y.; Zhang, D.; Mao, Z.; Lu, L.; Gao, C.; et al. Dimethyl Itaconate-Loaded Nanofibers Rewrite Macrophage Polarization, Reduce Inflammation, and Enhance Repair of Myocardic Infarction. *Small* **2021**, *17* (17), No. e2006992.
(16) Song, H.; Xu, T.; Feng, X.; Lai, Y.; Yang, Y.; Zheng, H.; et al. Itaconate prevents abdominal aortic aneurysm formation through inhibiting inflammation via activation of Nrf2. *EBioMedicine* **2020**, *57*, 102832.
(17) Bambouskova, M.; Potuckova, L.; Paulenda, T.; Kerndl, M.; Mogilenko, D. A.; Lizotte, K.; et al. Itaconate confers tolerance to late NLRP3 inflammasome activation. *Cell Rep.* **2021**, *34*, 108756.
(18) Tan, B.; Malu, S.; Roth, K. D. Development of ion pairing LC-MS/MS method for itaconate and cis-aconitate in cell extract and cell media. *J. Chromatogr. B: anal. Technol. Biomed. Life Sci.* **2020**, *1146*, 122120.
(19) Winterhoff, M.; Chen, F.; Sahini, N.; Ebensen, T.; Kuhn, M.; Kaever, V.; et al. Establishment, validation, and initial application of a sensitive LC-MS/MS assay for quantification of the naturally occurring isomers itaconate, mesaconate, and citraconate. *Metabolites* **2021**, *11*, 270.
(20) Qin, W.; Qin, K.; Zhang, Y.; Jia, W.; Chen, Y.; Cheng, B.; et al. S-glycosylation-based cysteine profiling reveals regulation of glycolysis by itaconate. *Nat. Chem. Biol.* **2019**, *15*, 983−991.
(21) Qin, W.; Zhang, Y.; Tang, H.; Liu, D.; Chen, Y.; Liu, Y.; et al. Chemoproteomic profiling of itaconation by bioorthogonal probes in inflammatory macrophages. *J. Am. Chem. Soc.* **2020**, *142*, 10894−10898.
(22) Sun, P.; Zhang, Z.; Wang, B.; Liu, C.; Chen, C.; Liu, P.; Li, X. A genetically encoded fluorescent biosensor for detecting itaconate with subcellular resolution in living macrophages. *Nat. Commun.* **2022**, *13* (1), 6562.
(23) Guberovic, I.; Frezza, C. Functional implications of fumarate-induced cysteine succination. *Trends Biochem. Sci.* **2024**, *49*, 775.
(24) Chen, F.; Elgaher, W. A. M.; Winterhoff, M.; Büssow, K.; Waqas, F. H.; Graner, E.; et al. Citraconate inhibits ACOD1 (IRG1) catalysis, reduces interferon responses and oxidative stress, and modulates inflammation and cell metabolism. *Nat. Metab.* **2022**, *4*, 534−546.
(25) Shi, X.; Zhou, H.; Wei, J.; Mo, W.; Li, Q.; Lv, X. The signaling pathways and therapeutic potential of itaconate to alleviate inflammation and oxidative stress in inflammatory diseases. *Redox Biol.* **2022**, *58*, 102553.
(26) Li, Z.; Zheng, W.; Kong, W.; Zeng, T. Itaconate: A potent macrophage immunomodulator. *Inflammation* **2023**, *46*, 1177−1191.
(27) Hamashima, Y.; Harter, J. G.; Coons, A. H. The localization of albumin and fibrinogen in human liver cells. *J. Cell Biol.* **1964**, *20*, 271−279.
(28) Roll, G. R.; Willenbring, H. Transplanted nonviable human hepatocytes produce appreciable serum albumin levels in mice. *Stem Cell Res.* **2010**, *5*, 267−270.
(29) Ma, B.; Ju, A.; Zhang, S.; An, Q.; Xu, S.; Liu, J.; Yu, L.; Fu, Y.; Luo, Y.; et al. Albumosomes formed by cytoplasmic pre-folding albumin maintain mitochondrial homeostasis and inhibit nonalcoholic fatty liver disease. *Signal Transduction Targeted Ther.* **2023**, *8* (1), 229.
(30) Feldmann, G.; Penaud-Laurencin, J.; Crassous, J.; Benhamou, J. P. Albumin synthesis by human liver cells: its morphological demonstration. *Gastroenterology* **1972**, *63*, 1036−1048.
(31) Hochman-Mendez, C.; Curty, E.; Taylor, D. A. Change the laminin, change the cardiomyocyte: Improve untreatable heart failure. *Int. J. Mol. Sci.* **2020**, *21*, 6013.
(32) Lumkwana, D.; Botha, A.; Samodien, E.; Hanser, S.; Lopes, J. Laminin, laminin-entactin and extracellular matrix are equally appropriate adhesive substrates for isolated adult rat cardiomyocyte culture and experimentation. *Cell Adh Migr.* **2018**, *12*, 503−511.
(33) Yap, L.; Tay, H. G.; Nguyen, M. T. X.; Tjin, M. S.; Tryggvason, K. Laminins in cellular differentiation. *Trends Cell Biol.* **2019**, *29*, 987−1000.
(34) Piper, H. M.; Jacobson, S. L.; Schwartz, P. Determinants of cardiomyocyte development in long-term primary culture. *J. Mol. Cell. Cardiol.* **1988**, *20*, 825−835.
(35) Cullen, J. M.; Stalker, M. J. *Liver and Biliary System. Jubb, Kennedy & Palmer's Pathology of Domestic Animals: Vol. 2*; Elsevier, 2016; pp. 258−352.e1.
(36) Vollmar, B.; Menger, M. D. The hepatic microcirculation: mechanistic contributions and therapeutic targets in liver injury and repair. *Physiol. Rev.* **2009**, *89*, 1269−1339.
(37) Stanger, B. Z. Cellular homeostasis and repair in the mammalian liver. *Annu. Rev. Physiol.* **2015**, *77*, 179−200.
(38) Strelko, C. L.; Lu, W.; Dufort, F. J.; Seyfried, T. N.; Chiles, T. C.; Rabinowitz, J. D.; et al. Itaconic acid is a mammalian metabolite induced during macrophage activation. *J. Am. Chem. Soc.* **2011**, *133*, 16386−16389.
(39) Liu, D.; Xiao, W.; Li, H.; Zhang, Y.; Yuan, S.; Li, C.; et al. Discovery of itaconate-mediated lysine acylation. *J. Am. Chem. Soc.* **2023**, *145*, 12673−12681.
(40) Sakai, A.; Kusumoto, A.; Kiso, Y.; Furuya, E. Itaconate reduces visceral fat by inhibiting fructose 2,6-bisphosphate synthesis in rat liver. *Nutrition* **2004**, *20*, 997−1002.
(41) Ma, E.; Xing, H.; Pei, J.; Zhang, Q.; Li, R.; Shen, C.; et al. Itaconic acid facilitates inflammation abatement and alleviates liver ischemia-reperfusion injury by inhibiting NF-κB/NLRP3/caspase-1 inflammasome axis. *Ann. Transl. Med.* **2022**, *10*, 861.
(42) Shan, Q.; Li, X.; Zheng, M.; Lin, X.; Lu, G.; Su, D.; et al. Protective effects of dimethyl itaconate in mice acute cardiotoxicity induced by doxorubicin. *Biochem. Biophys. Res. Commun.* **2019**, *517*, 538−544.
(43) Song, J.; Zhang, Y.; Frieler, R. A.; Andren, A.; Wood, S.; Tyrrell, D. J.; et al. Itaconate suppresses atherosclerosis by activating a Nrf2-


https://doi.org/10.1021/acsomega.4c08552
*ACS Omega* 2025, 10, 1110−1121

dependent antiinflammatory response in macrophages in mice. *J. Clin. Invest.* **2024**, *134*, 134.
(44) Diotallevi, M.; Ayaz, F.; Nicol, T.; Crabtree, M. J. Itaconate as an inflammatory mediator and therapeutic target in cardiovascular medicine. *Biochem. Soc. Trans.* **2021**, *49*, 2189−2198.
(45) Cyr, Y.; Bozal, F. K.; Durán, J. G. B.; Newman, A. A. C.; Amadori, L.; Smyrnis, P.; Gourvest, M.; Das, D.; Gildea, M.; Kaur, R.; Zhang, T.; et al. The IRG1−itaconate axis protects from cholesterol-induced inflammation and atherosclerosis. *Proc. Natl. Acad. Sci. U. S. A.* **2024**, *121* (15), No. e2400675121.
(46) Hong, N. E.; Chaplin, A.; Di, L.; Ravodina, A.; Bevan, G. H.; Gao, H.; et al. Nanoparticle-based itaconate treatment recapitulates low-cholesterol/low-fat diet-induced atherosclerotic plaque resolution. *Cell Rep.* **2024**, *43*, 114911.
(47) Rathjen, D. A.; Geczy, C. L. Conditioned medium from macrophage cell lines supports the single-cell growth of hybridomas. *Hybridoma* **1986**, *5*, 255−261.



https://doi.org/10.1021/acsomega.4c08552
*ACS Omega* 2025, 10, 1110−1121